

Received April 5, 2021, accepted April 25, 2021, date of publication April 27, 2021, date of current version May 4, 2021.

Digital Object Identifier 10.1109/ACCESS.2021.3076111

Performance Improvement of Dual Stator Axial Flux Spoke Type Permanent Magnet Vernier Machine

MUHAMMAD BILAL¹, JUNAID IKRAM¹, ADNAN FIDA¹,
SYED SABIR HUSSAIN BUKHARI^{2,3}, NADEEM HAIDER¹,
AND JONG-SUK RO^{3,4}

¹Department of Electrical and Computer Engineering, COMSATS University Islamabad, Islamabad 45550, Pakistan

²Department of Electrical Engineering, Sukkur IBA University, Sukkur 65200, Pakistan

³School of Electrical and Electronics Engineering, Chung-Ang University, Seoul 06974, South Korea

⁴Department of Intelligent Energy and Industry (BK4), Chung-Ang University, Seoul 06974, South Korea

Corresponding author: Jong-Suk Ro (jongsukro@gmail.com)

This work was supported in part by the Basic Science Research Program through the National Research Foundation of Korea by the Ministry of Education under Grant 2016R1D1A1B01008058, and in part by the Brain Pool (BP) Program through the National Research Foundation of Korea (NRF) by the Ministry of Science and ICT under Grant 2019H1D3A1A01102988.

ABSTRACT This paper presents performance improvement of dual stator axial-flux spoke type permanent magnet vernier machine (DSAFST-PMVM), which has the capability to generate high torque at a lower speed due to magnetic gearing effect. Flux focusing effect is created by means of dual stator single rotor topology with spoke type permanent magnets. It is best suitable for high-performance industrial applications such as servo motors, robot arms, wind power, electric vehicles, and elevator applications. A PM shape is proposed in this paper which has notches in such a way that it produces discrete skew effect which reduces the cogging torque and torque ripples. Optimization of magnet shape is done to make the optimized model more competitive than the proposed and basic models. Main parameters such as back emf, cogging torque, torque ripples, electromagnetic torque, VTHD, airgap flux densities, flux density distribution, power factor, and power of the machine are compared among the basic model, proposed model, and optimized models. The comparative analysis is done by using the time stepped 3D finite element method.

INDEX TERMS Axial flux, cogging torque, dual stator axial flux machine, flux focusing effect, magnetic gearing effect, torque ripples, vernier machine, finite element method.

I. INTRODUCTION

Investigations on permanent magnet machines at a massive scale have commenced with the evolution of permanent magnet material [1]. These PM machines have better efficiency and high-power density, due to which they are superior from most of the electromechanical applications such as induction motors and DC motors. In recent years, permanent magnet machines are gaining popularity in the field of direct drive systems because of their enhanced efficiency and high-power density with minimal losses. These characteristics make them the best choice for the direct drive system [2]. When the motor is directly connected to load with high torque at low speed, then the direct drive system came into being. In earlier times,

the motor is not directly connected to the low-speed load. The gear mechanism is used in between the motor and low-speed load to sustain higher torque, but these mechanical gears have wear and scratch as well as gear transmission losses. Moreover, require regular maintenance and extra space for installation [3], [4]. However, with direct drive systems, existing topologies required larger dimensions as material consumption increased. This requires a compromise between the omission of the gear mechanism and the bulky size of the machine. Therefore, much of the work on machinery is focused on direct drive machines to replace the classic gear mechanism [5]–[10]. Many new prototypes have been proposed for this purpose in recent years. For example, a transverse permanent magnet machine is known for its excessive torque density, but it has a complex arrangement with a very low power factor and high cogging torque [11], [12].

The associate editor coordinating the review of this manuscript and approving it for publication was Sonia F. Pinto¹.

Furthermore, a method of integrating coaxial magnetic gear in PM motors has also been introduced. For this purpose, the brushless outer rotor PM machine may be merged with a coaxial magnetic gear to share a single rotor to form a magnetic gear machine. This concept enables direct drive systems that reduce the requirement, intended for mechanical gear, and improve high efficiency and ruggedness. Magnetic gear machines, however, require two rotors whose alignment and precision are very complex, growing the worth and complexity of production [13], [14].

Permanent magnet (PM) is improved by increasing the energy creation of the permanent magnet material. As a unique electromechanical device, a permanent magnet vernier machine offers all the benefits of vernier and permanent magnet machines (PMVM) [15], [16]. As a PMVM design principle, the number of PM poles is not equivalent to the number of winding poles and does not correspond to the conventional PM machines to achieve the so-called “magnetic gear effect”. When the number of flux modulators (ferromagnetic poles) is equal to the number of stator tooth and stator tooth act as flux modulator, resulting in complete removal of flux modulator from the machine, then the topology is called PMVM. PMVM has high torque density and small size as compared to traditional permanent magnet machines with the same ratings. This high torque characteristic is due to the flux modulation effect and is considered to be the best substitute aimed at low-speed direct-drive systems [8], [15], [17], [18]. Because of the fact, PM vernier machines are generally designed with large numbers of magnetic poles, making them suitable for generating high torque at relatively low speeds. Therefore, no reduction gear is required, which requires a clearance, friction loss, and maintenance. A higher torque density should be considered for the topology design to achieve competitive machine performance. However, when compared to a conventional PM machine, a normal VPM machine will experience a low power factor characteristic [11], [19]–[20]. which will increase the converter rating of the VPM machine for a given output power, which will be costly and require a high rating converter. Therefore, methods to upgrade the power factor of VPM machines are motivating. The dual stator axial flux spoke type permanent magnet vernier machine (DSAFST-PMVM) topology has been proven with high torque density and enhanced power factor related to conventional PMVM machines [21].

The torque of an electrical machine is the combination of constant component and periodic component. The periodic component is related to the rotor position and is dominant over the constant component. The pulsation in the torque, also called torque ripples are due to the periodic component. Torque ripples depend upon three things, which are the root causes: (a) cogging torque which is defined as the interaction among PM of the rotor and the teeth of the stator. The physical distance between teeth of the stator and PM of the rotor is less so the force of attraction increased at that point and torque is produced with the symptom of jerkiness, (b) non-sinusoidal

distribution of magnetic flux density in the air gap, and (c) unequal permeances [22]. Torque ripples and cogging torque are more dominant at low speed. At high speed, the torque ripples are filtered out due to the moment of inertia. There are different techniques available for cogging torque minimization, for instance, contouring the slots and magnets, shaping the magnets, the introduction of dummy slots, effective ratio of magnet pole arc to pole pitch, fractional winding, and reduce the slot area [23]. DSAFST-PMVM has low inertia and high torque density make it very attractive for high-performance industrial applications such as servo motors, robot arms, wind power, electric vehicles, and elevator applications. In these applications, the torque should be as smooth as attainable to skip vibrations, so it is usually considered to have a minimal torque ripple.

The paper is divided into three sections. In the first section, DSAFST-PMVM is analyzed and consider as a basic model, in the second section we proposed a new magnet shape and refer it as a proposed model, also compare its performance with the basic model. In the last section, we optimized the magnet shape to develop an optimized model for competitive analysis.

II. DUAL STATOR AXIAL-FLUX SPOKE TYPE PERMANENT MAGNET VERNIER MACHINE

A. OPERATION

The operating principle of PMVM is almost the same as magnetic gear and magnetically geared machines. High and low pace rotors of magnetic gear are correlated to stator and rotor poles of PMVM, correspondingly. Its number of stator tooth is equal to the sum of rotor permanent magnet pole pairs and winding pole pairs, which means that the number of rotor permanent magnet pole pairs are greater than the number of stator winding pole pairs [13], [20], [21], [24]. Consequently, it breaks the conventional rule of the equal number of rotor permanent magnet pole pairs and winding pole pairs. Despite unequal pole pair number of stator and rotor, PMVM yet attains the steady torque by synchronizing the stator MMF to air gap flux rotation because of flux modulation effect by the stator tooth. Design rule for PMVM is discussed in [25]–[27] which is:

$$Z_r = Z_s \pm p \quad (1)$$

where Z_r represents the PM pole pair, Z_s is the slot number (number of flux modulator) and p is stator winding pole pairs. In other words, the required low-speed high-torque attribute in a PMVM is fetched out by the magnetic gearing effect, in such a way that a minor mobility of the rotor conveys an enormous flux variation [21]. Z_r is normally designed much larger than p in PMVMs. Once the flux rotates 360° , the rotor only rotates by $360^\circ/Z_r$ as expressed in equation (2). where ω_r rotor speed, ω_{MMF} flux speed, τ_r rotor slot pitch, and τ_{MMF} MMF pole pitch

$$\frac{\omega_r}{\omega_{MMF}} = \frac{\text{Rotor speed}}{\text{Rotating Field Speed}} = \frac{\tau_r}{\tau_{MMF}} = \frac{p}{Z_r} \quad (2)$$

B. CONFIGURATION

The configuration of DSAFST PMVM is shown in Fig. 3. Two half-slot-pitch shift stators perpendicular to spoke magnet and air gap of the rotor. A rotor pole directs the flux over the two air gaps to the two stator cores, the pitch being shifted by half a slot. The flux moves in a stator core in the circumferential direction and back through the air gap to the rotor and into another air gap to the other stator core. The tooth of the first stator faces the slot of the second stator creates unalignment which directs the flux to flow over the entire machine which is different from conventional surface type machines. In conventional surface type machines, the flux loop cover half of the machine. This unaligned two stator arrangement inherently produces a skew effect which lessens machine cogging torque. Conductors of coils are wrapped over the stator yoke to apply drum winding in the open slot arrangement as shown in Fig. 4. The main design parameters of DSAFST-PMVM are tabulated in Table. 1. Magnet pieces with a 7 mm thickness are selected in event of demagnetization. A ratio of stator slot width per slot pitch 0.63 is picked as a result of the optimized design of the open slot in PMVM [28].

C. FLUX FOCUSING

The DSAFST PMVM design uses spoke-arranged magnets to have a flux-focusing effect, thus raising the useful magnet flux. The rotor pole directs flux through both the outer and inner airgaps with half teeth pitch shifted dual stators, as seen in Fig. 1. Circumferentially, the flux flows through one stator core, back through the air gap through the rotor, and then across another air gap through the other stator core. Figure 1 (a) and (b) display the flux line in two distinct relative positions. The magnet’s length can be varied to achieve the desired flux focusing.

Fundamental section of machine, which consist of only one tooth, one slot and one magnet pole pair is shown in Fig. 2. The specific arrangement of PMs in Fig.2 (a) and (b) illustrated that Spoke type PMVM topology discourage flux leakage between adjacent PM. Thus, large leakage flux in Surface PMVM result in poor power factor.

Above discussion shows that this topology can enhance the air gap flux density and useful magnet flux. Due to which few ampere-turns are required for desired Output power. Therefore, the winding reactance can be largely decreased which improve the power factor of this topology.

D. DESIGN EQUATIONS

The designing of the PMVM is done in [21], [29], in which the magnetic field is analyzed by taking a small section of the DSAFST-PMVM, which includes single pole pair, slot, and tooth. Equation (1-16) are basic design equations presented in [21], [29], for dual stator axial flux topology of PMVM. All the machines in this paper follow the same design equations.

From equation (1), we have the number of combinations for rotor pole pair and the number of slots of the

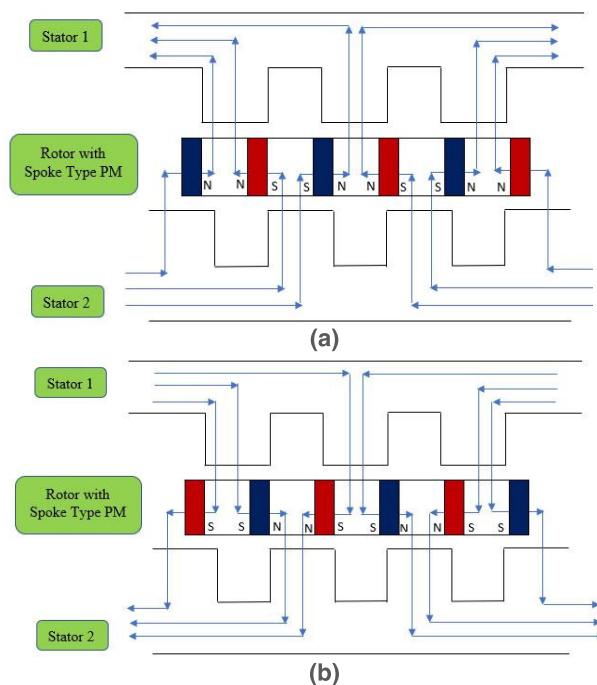


FIGURE 1. Flux path of DSAFST-PMVM with respect to rotor positions. (a) Position 1. (b) Position 2: Rotated by one rotor pole pitch.

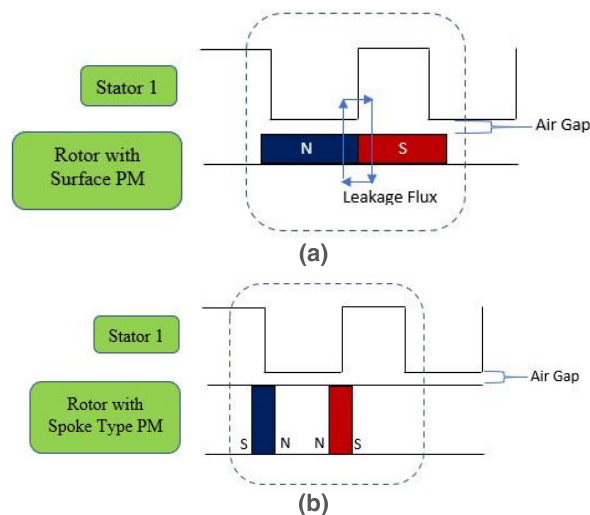


FIGURE 2. Fundamental section of machine (a) Surface PMVM (b) Spoke Type PMVM.

DSAFAST-PMVM. One selection is adopted for all the machines analysis. $Z_r = 17$, $Z_s = 18$ and $p = 1$.

For a 3-phase machine (m),

$$q = \frac{Z_s}{2pm} = 3 \tag{3}$$

The slot per pole per phase is illustrated in Fig.4. Axial field permeance coefficient P is given by:

$$P(\theta) = P_0 + (-1)^j \sum_{m=1}^{\infty} P_m \cos(mZ_s\theta) \tag{4}$$

$$P_0 = \frac{\mu_0}{g_e} = \frac{\mu_0}{k_{cs}k_{cr}g}k_{co} = \frac{\mu_0}{k_{cs}k_{cr}g}(1 - 1.6\beta\frac{b_o}{\tau_s}) \quad (5)$$

$$P_1 = \frac{2\mu_0\beta}{\pi g} \sin(1.6\pi\frac{b_o}{\tau_s}) \frac{1}{1 - 1.6^2(\frac{b_o}{\tau_s})^2} \quad (6)$$

$$k_{cs} \approx \frac{\tau_s}{\tau_s - \frac{b_o^2}{5g+b_o}} \quad (7)$$

$$k_{cr} \approx \frac{\tau_r}{\tau_r - \frac{g_m^2}{5g+g_m}} \quad (8)$$

P_0 is an average air gap permeance coefficient,
 P_m is the amplitude of the permeance coefficient (m_{th} harmonic),

k_{cs} , and k_{cr} are the Carter coefficients,

j is the number of slot shifts of the short pitch windings,

μ_0 is the permeability of air,

g_e is the equivalent airgap length,

g is the mechanical airgap length,

g_m is the width of PM,

b_0 is slot width,

k_{c0} is a coefficient linked to airgap and slot,

β is a function of the ratio b_0/g ,

τ_s is stator pole pitch,

τ_r is rotor pole pitch.

Applying the law of the Ampere and ignoring the drop of MMF in the core to get the fundamental amplitude of airgap MMF $F_{gap}(\theta)$ as observed in (9)-(13). MMF F_{gapm} cannot be ignored as PM relative permeability is near to one.

F_m is the MMF through PM,

F_{gap1} and F_{gap2} correspond to the MMF drops in two airgaps,

F_{gap} shows their average value.

$$F_{gap1} + F_{gap2} + F_{gapm} + F_m = 0 \quad (9)$$

$$F_m = \pm \frac{B_r g_m}{\mu_m} \quad (10)$$

$$\frac{F_{gap}}{F_{gapm}} = \frac{(F_{gap1} + F_{gap2})/2}{F_{gapm}} = \frac{4/(P_o \tau_r l_{stk})}{g_m/(\mu_o h_m l_{stk})} = \frac{P_o g_m}{4h_m \mu_o} \tau_r \quad (11)$$

$$F_{gap} = \frac{\frac{B_r g_m}{\mu_m}}{2 + \frac{P_o g_m}{4h_m \mu_o} \tau_r} \quad (12)$$

By applying Fourier series, it yields to,

$$F_{gap}(\theta) = \frac{4}{\pi} F_{gap} \sum_{n=1, odd}^{\infty} \frac{1}{n} \cos(nZ_r(\theta - \theta_m)) \quad (13)$$

B_r is residual flux density,

μ_m is the permeability of PM,

l_{stk} is stack length,

h_m is rotor height.

The flux density is created by that of the MMF and permeance, so given the main order of components $m = 0, 1$, and $n = 1$, no-load flux density throughout the airgap $B_{PM}(\theta)$ is

displayed here below:

$$\begin{aligned} B_{PM}(\theta) &= F_{gap}(\theta)P(\theta) \\ &\approx \frac{4}{\pi} F_{gap} \cos Z_r(\theta - \theta_m)(P_o + (-1)^j P_1 \cos(Z_s \theta)) \\ &\quad + B_{har} \\ &= \frac{4}{\pi} F_{gap} P_o \cos(Z_r(\theta - \theta_m)) \\ &\quad + (-1)^j \frac{2}{\pi} F_{gap} P_1 \cos(Z_r - Z_s)\theta - Z_r \theta_m \\ &\quad + B_{har} \\ &= B_{PMO} \cos(Z_r(\theta - \theta_m) + (-1)^j B_{PM1} \\ &\quad \times \cos(Z_r - Z_s)\theta - Z_r \theta_m) + B_{har} \end{aligned} \quad (14)$$

B_{har} represents the harmonic component. For back-EMF, considering only the flux components of its low order,

$$\begin{aligned} e(t) &= \frac{d\lambda(\theta)}{dt} = \pi N D_g l_{stk} \omega \sum_{k=0}^{q-1} \int_{ka}^{\pi/p+ka} B_{PM}(\theta) d\theta \\ &= k_s N D_g l_{stk} \omega (B_{PMO} \pm (-1)^j \frac{Z_r B_{PM1}}{2p}) \cos(z_r \theta_m \pm p\theta) \end{aligned} \quad (15)$$

λ is phase flux linkage,

N is the number of turns (one phase),

D_g is airgap diameter,

ω is mechanical velocity,

α is slot span and defined as $2\pi/Z_s$

k_s is the winding factor.

$$T = e_a i_a + e_b i_b + e_c i_c / \omega \quad (16)$$

e_a, e_b, e_c are back-EMF (rms value),

i_a, i_b, i_c are excitation current (rms value).

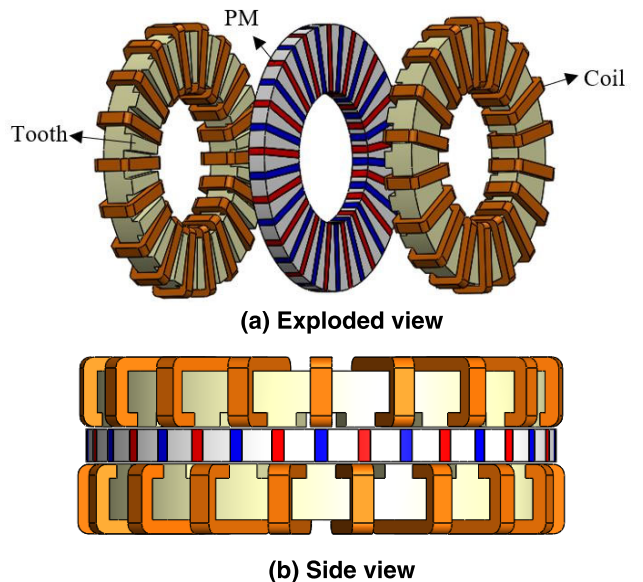


FIGURE 3. Configuration of the DSAFST-PMVM.

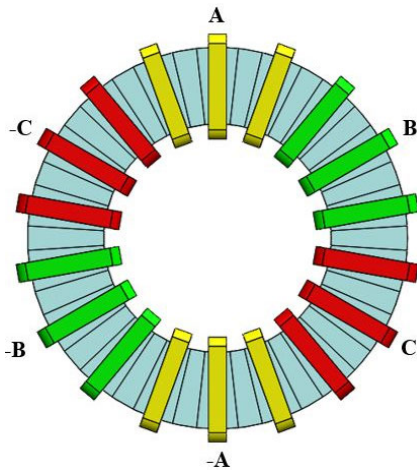


FIGURE 4. Drum winding.

E. ANALYSIS

DSAFST-PMVM has high back emf at low speed of 300 rpm due vernier effect and required a smaller number of amperes turns as compared to conventional axial flux machines of the same size. DSAFST-PMVM has 120 (peak-to-peak) voltages with sinusoidal waveform is clearly shown in Fig. 9. Cogging torque has also been tested in no-load condition since it is the torque due to the interaction among rotor PMs and slots of the stator. 3D-FEM analysis of cogging torque waveform is presented in Fig. 10. The peak-to-peak values of the cogging torque waveform are not the same, Negative maximum value is -6.02 N-m while the positive maximum peak is 5.08 N-m.

TABLE 1. Specifications of the DSAFST-PMVM.

Items	Unit	DSAFST-PMVM
Power	kW	6.4
Current density	A/mm ²	4.4
Rated speed	rpm	300
Winding pole pair number <i>p</i>	-	1
No. of slots <i>Z_s</i>	-	18
No. of magnet pole pair <i>Z_r</i>	-	17
No. of coils	-	18
Stator outer diameter <i>D_o</i>	mm	254
Stator inner diameter <i>D_i</i>	mm	152
Axial length <i>l</i>	mm	82.4
Air gap <i>g</i>	mm	1.2
PM thickness <i>g_m</i>	mm	7
Magnet (NdFeB)	-	<i>B_r</i> =1.23T, <i>H_c</i> =-890kA/m

DSAFST-PMVM has a high average torque of 188.76 N-m at a very small outer diameter of 262.4 mm due to the magnetic gearing effect. Which builds DSAFST-PMVM high torque density machine. 3D-FEM analysis of output torque of DSAFST-PMVM is displayed in Fig. 11 with maximum current (RMS) of 26 A is supplied. Due to the high airgap flux density of DSAFST-PMVM, end turns are effectively utilized which enhances the torque profile. With the effect of flux modulation and flux focusing, the air gap flux density

of DSAFST-PMVM is highly enhanced, which enables the DSAFST-PMVM to deliver high power. High air gap flux density also enables the machinery to provide the required power at fewer ampere-turns due to which winding reactance is highly decreased. Which significantly decreased the unwanted losses. Furthermore, less winding reactance also improves the power factor of the machine. Flux focusing effect significantly decreased leakage flux, consequently, the power profile of DSAFST-PMVM is highly enhanced. 3D FEA simulation results of the DSAFST-PMVM are shown in Fig. 12.

Stator and rotor are made from non-oriented silicon steel (50JNE350), which has good performance at high and medium-range frequencies. Magnetic flux density distributions without load (by PMs) are shown in Fig. 5. In this machine stator and rotor is of 1.75 T out of material saturation which is up to the mark. Flux density distribution clearly illustrates that it has 2 winding poles. Via flux focusing effect, spoke arranged PM provides a greater flux density nevertheless along with gigantic harmonics in one airgap. Fig. 14 defines the average radius in one airgap which noticeably displays the peak value of 1.5 T, which proves the presence of flux focusing effect. Fig. 6 shows fast Fourier transform (FFT) results for each harmonic component of the airgap flux density, where the magnet pole pairs number *Z_r* = 17 is the fundamental harmonic order, with one rotor pole pair number (17+1), the 35th is the working harmonic.

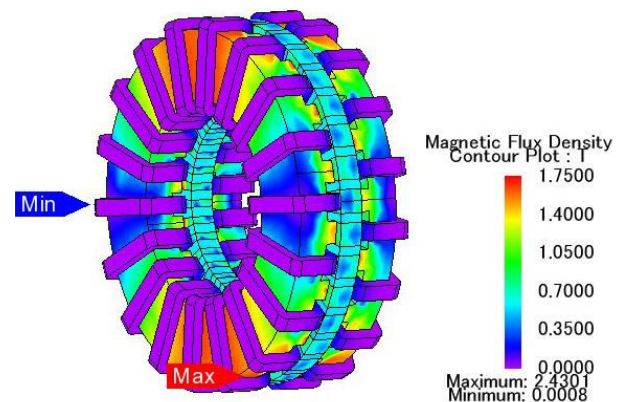


FIGURE 5. Flux density distribution of basic model.

III. PROPOSED NOTCHED SHAPE MAGNET

Cogging torque is directly proportional to the square of the air gap flux and change in reluctance w.r.t rotor position. Mathematically it can be symbolized as below.

$$T_{cog} = -\frac{1}{2} \phi_g^2 \frac{dR}{d\theta} \tag{17}$$

where ϕ_g is the air-gap flux, R is the air-gap reluctance, and θ is the position of the rotor.

Equation (17) gives the concept that cogging torque is the interaction among the rotor PMs (the cause of the air-gap flux then cogging torque is studied with an unexcited stator) and the teeth of the stator (the cause of the varying

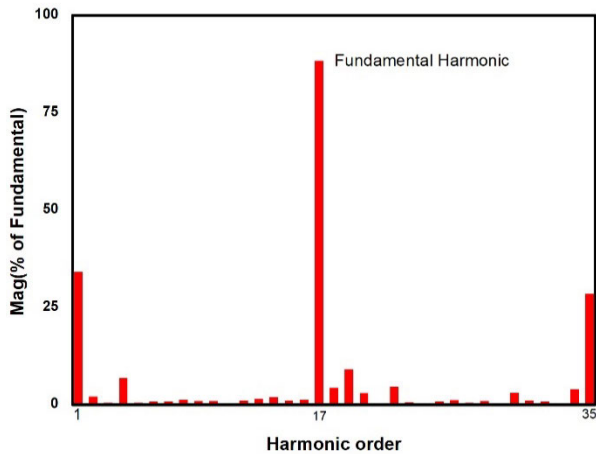


FIGURE 6. FFT results of airgap flux density waveform.

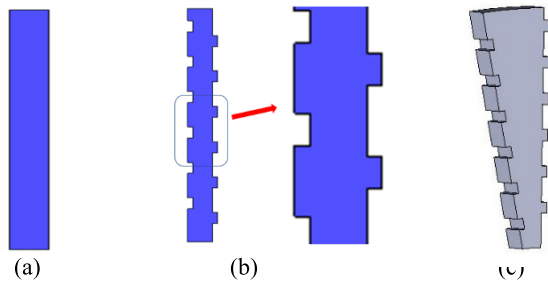


FIGURE 7. PM and rotor core shape. (a) Conventional rectangular shape PM (b) Proposed notched shape PM (c) Rotor segment of proposed model.

air-gap reluctance). This equation specifies that either airgap magnetic flux or reluctance variation need to be lessened to minimize cogging torque. Though reducing airgap magnetic flux worsens motor performance and therefore it is not a feasible tactic to minimize cogging torque. Hence, reducing the reluctance variation is an appropriate way to lessen the cogging factor.

Skewing magnets or shaping magnets certainly decrease this variation and thus reduce cogging. Both the peak value and shape of the cogging topography rely on the physical geometry of the magnet. The conventional rectangular shape magnet and proposed notched shape magnet is shown in Fig. 7, for fair comparison the volume of both magnets is kept constant. The proposed magnet has notches on one side but adding the same size of space on the other side of the magnet to keep the volume of the magnet constant. The proposed notched shaped magnet has a built-in characteristic of skew effect, which reduce the cogging torque. Basically, the skew effect has two types, continuous and discrete skew as displayed in Fig. 8.

The magnets are circumferentially magnetized for flux focusing effect so the rotor segments are directly involved in the flux path or we can say that the rotor segment links the flux to stator winding axially. Because of the proposed magnet shape geometry, the shape of the rotor segment is changed as shown in Fig. 7(c). The new shape of the rotor segment

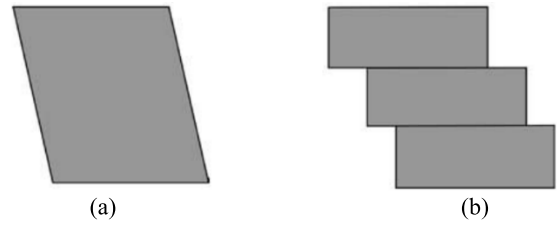


FIGURE 8. Basic types of skew effect (a) continuous (b) discrete.

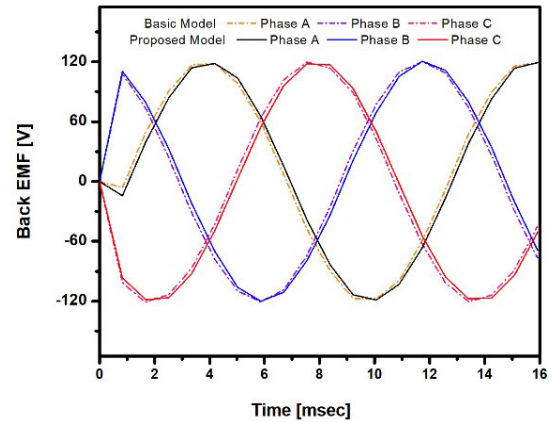


FIGURE 9. Back EMF assessment of basic model and proposed model.

has a discrete skew effect. If we divide the rotor segment into the number of identical slices. Then each slice experiences a minor skew effect. Although it is not a pure discrete skew effect, but this factor plays role in the reduction of cogging torque in the proposed model. From equation (17), the factor $dR/d\theta$ is minimum in the proposed notched shape magnet due to the built-in characteristic of discrete skew effect while it is maximum in conventional rectangular shape magnet.

$$\frac{dR}{d\theta}(\text{Proposed}) < \frac{dR}{d\theta}(\text{Conventional}) \quad (18)$$

Considering these factors, the order of cogging torque of proposed magnet shape and conventional rectangular shape magnet is as follow:

$$T_{cog}(\text{Proposed}) < T_{cog}(\text{Conventional}) \quad (19)$$

In this paper, the conventional rectangular shape magnet model is specified as the basic model, which is discussed earlier in detail. In this section, we will compare the different parameters of both the basic and proposed models. Back EMF of the basic model and proposed model is presented in Fig. 9. The back EMF of the basic model and proposed model is $84.56 V_{rms}$ and $84.02 V_{rms}$ respectively. There is a negligible reduction of voltages in the proposed model as compared to the basic model, but the back EMF of the proposed model has less percentage of harmonics. VTHD of the basic model and proposed model is 0.67004% and 0.6678% respectively as shown in Fig. 15. The proposed magnet shape plays the role to minimize the harmonics, as sinusoidal flux density distribution depends upon it.

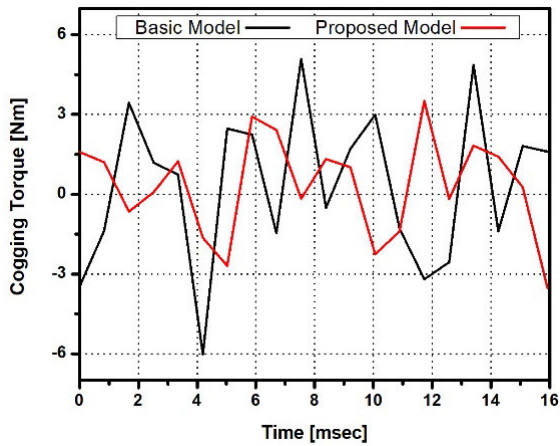


FIGURE 10. Cogging torque assessment of the basic and proposed models.

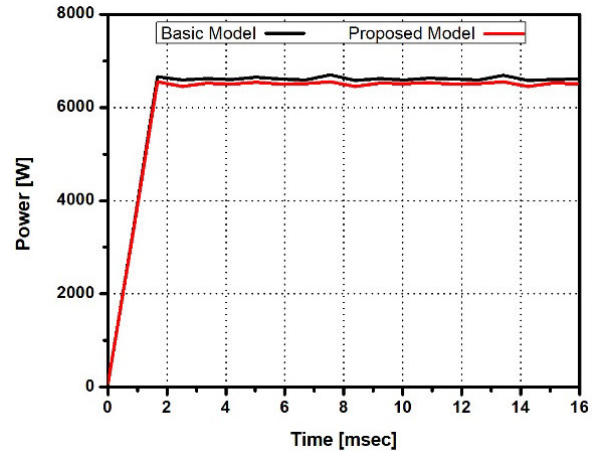


FIGURE 12. Power comparison of the basic and proposed models.

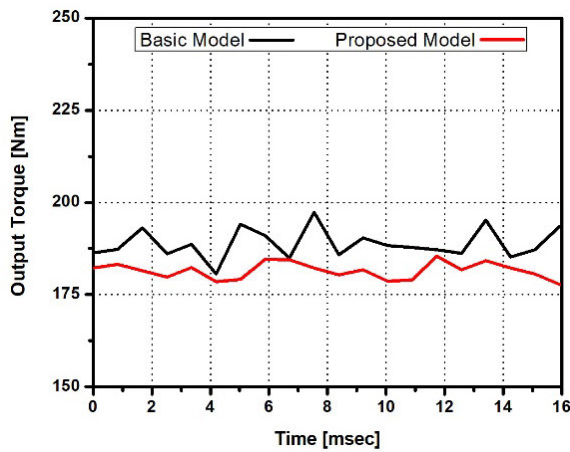


FIGURE 11. Output Torque assessment of the basic and proposed models.

The peak-to-peak cogging torque of the proposed model is 7.03 Nm, which is less than 11.1 Nm of the basic model due to the proposed magnet shape as shown in Fig. 10. There is a 36.67 % reduction in cogging torque with almost the same back EMF. The output torque of the basic model is 188.76 Nm while that of the proposed model is 181.55 Nm as shown in Fig. 11. The output torque of the basic model is slightly greater than the proposed model’s output torque but with a high percentage of torque ripples (8.82%). The torque ripples in the proposed model are 4.22%, which is the primary objective of this paper, to reduce torque ripples. The basic model has slightly greater power as compared to the proposed model as shown in Fig. 12.

Fig. 13 shows the flux density distribution of the proposed model with rated 4.4 A. The core of the proposed model is a maximum of 1.75 T to elude saturation factor. Air gap flux densities of the basic and proposed model are almost the same as shown in Fig. 14.

IV. MAGNET SHAPE OPTIMIZATION

The flow chart of the optimization procedure is shown in Fig. 16. First, design variables and objective function are

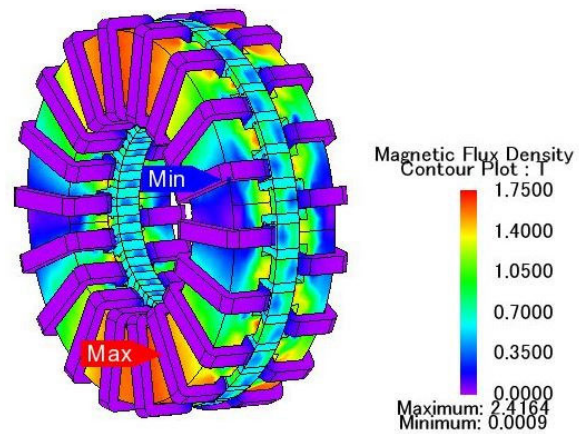


FIGURE 13. Flux density distribution of proposed model.

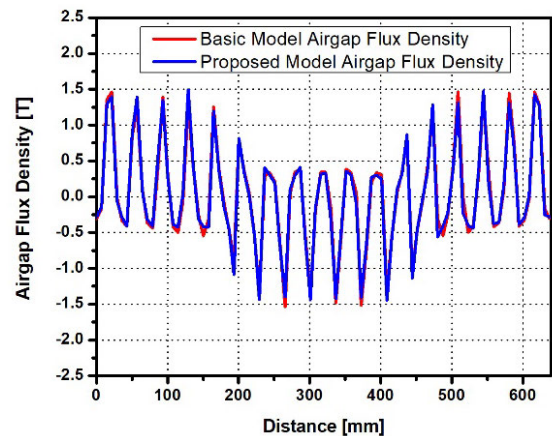


FIGURE 14. Airgap flux density at the average radius.

nominated. In the next phase, sampling is done to design the experiments by using the Latin hyper cube (LHC) sampling technique. Then to approximate the objective function, the kriging method is applied. The optimal value for the selected design variable is obtained through the genetic algorithm (GA). In the last phase, 3D FEM is performed to verify the output of the proposed machine.

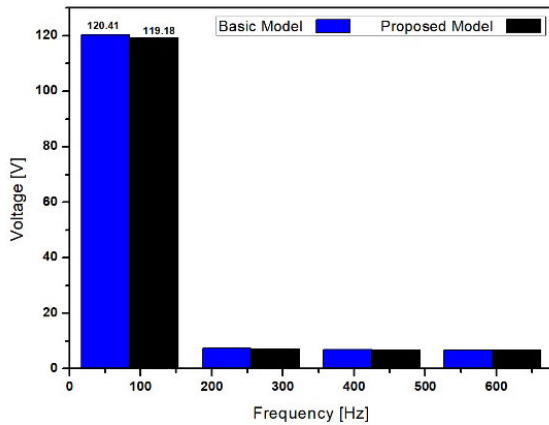


FIGURE 15. VTHD comparison of the basic and proposed models.

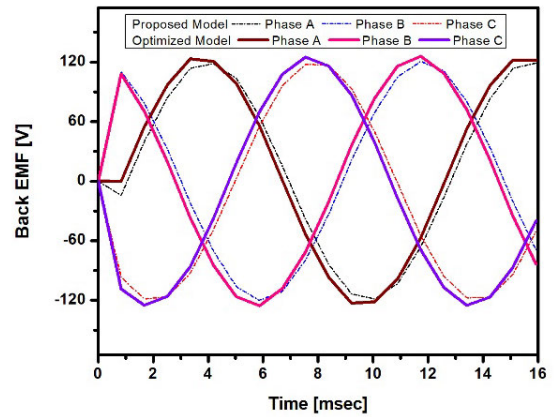


FIGURE 18. Back EMF assessment of the proposed and optimized models.

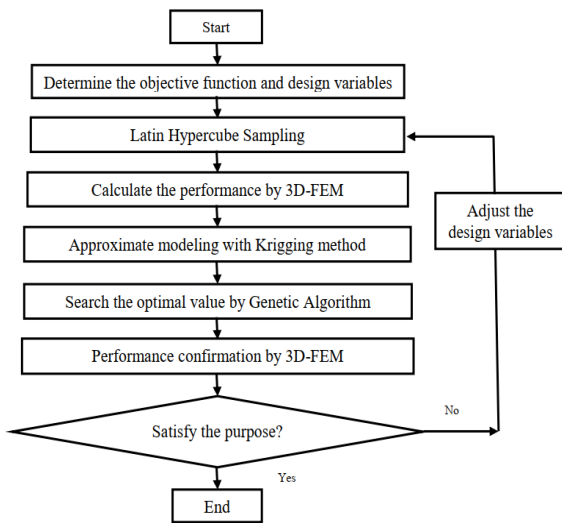


FIGURE 16. Optimization process.

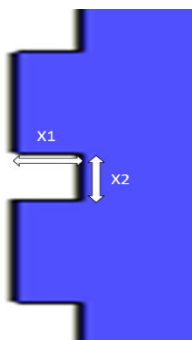


FIGURE 17. Proposed notched shape magnet.

A simple notched shape magnet as shown in Fig. 7(b), was chosen as the beginning point for optimization of the rotor pole. Length and width of notch illustrated as X1 [0.5-3.5 mm] and X2 [0.5-5 mm], respectively in Fig. 17, were chosen as the design variables. Each notch is just like a small rectangle, so we select any two sides X1 and X2 as design variables. The length and width of both variables must

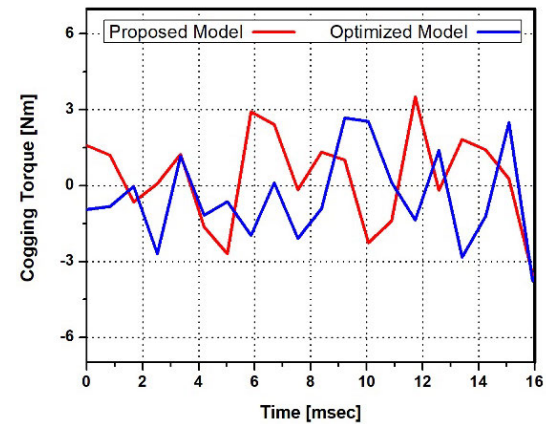


FIGURE 19. Cogging torque assessment of the proposed and optimized models.

be greater than 0 mm to create a notch as well as for a significant notch it must be at least 0.5 mm. The maximum length is equal to half of the magnet width which is $7/2 = 3.5$ mm, greater than half of the magnet will change its overall basic rectangular shape. For a given number of notches, the width should not be greater than 5 mm.

Objective Function:

Maximize the Back EMF

Minimize the cogging torque (pk-pk)

Selected Variables:

X1: Length of notch [0.5-3.5 mm]

X2: Width of notch [0.5-5 mm]

Optimal values:

X1 = 2.053 mm

X2 = 1 mm

Back EMF of the proposed model and optimized model is shown in Fig. 18, having a magnitude of $84.02 V_{rms}$ and $87.31 V_{rms}$, respectively. VTHD is improved from 0.6704 to 0.6601 by optimization of magnet shape as shown in Fig. 22. With the optimization of magnet shape, the back EMF of the optimized model is increased, and cogging torque is reduced by 8.53% as shown in Fig. 19, without compromising other parameters. The torque of the proposed model is 181.55 Nm

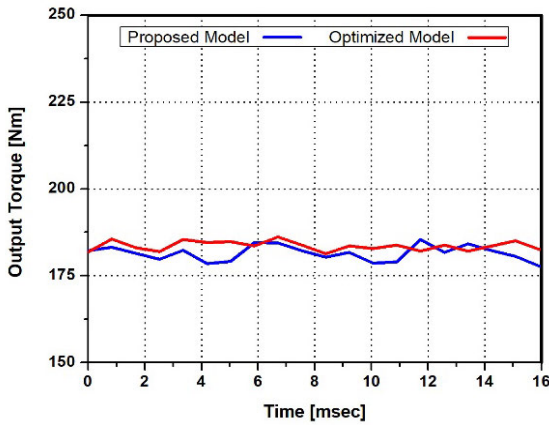


FIGURE 20. Output torque assessment of the proposed and optimized models.

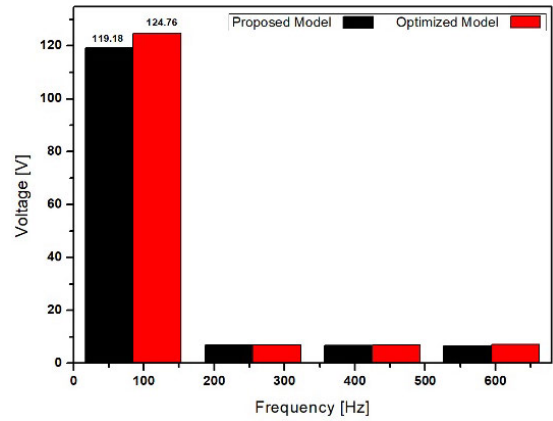


FIGURE 22. VTHD assessment of the proposed model and optimized models.

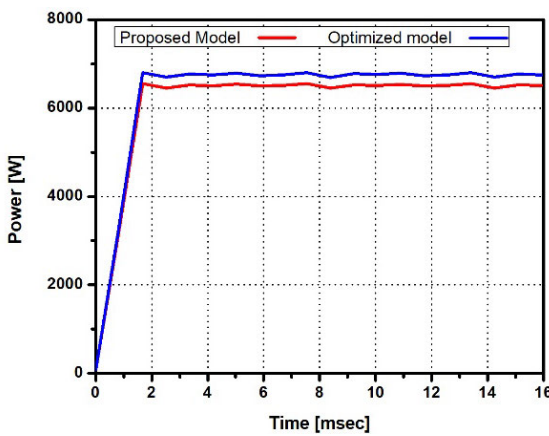


FIGURE 21. Power assessment of the proposed and optimized models.

TABLE 2. Comparison of 3D FEA results.

Items	Unit	Basic Model	Proposed Model	Optimized Model
Back EMF	V	84.56	84.02	87.31
Cogging torque	Nm (pk-pk)	11.1	7.03	6.43
Output torque	Nm	188.76	181.55	184.18
Torque ripples	%	8.82	4.22	3.93
Power	kW	6.2	6.1	6.3
VTHD	%	0.6704	0.6678	0.6601
Power factor	-	0.87	0.83	0.88

while that of the optimized model is 184.18 Nm as shown in Fig. 20.

Power profile is improved with optimization due to an increase in back EMF as shown in Fig. 21. Performance evaluation of basic, proposed, and optimized model is presented in Table 2. Chief problem of low power factor (0.3-0.5) of PMVM is removed by DSAFST-PMVM topology [19], [21]. It is improved to a remarkable level of 0.88. It is due to the

circumferentially magnetized spoke type PMs creating flux focusing and reducing leakage flux. Specific arrangement and direction of PMs decrease the leakage flux between the neighboring PMs and provide almost full utilization of PMs material. which results in increase in airgap flux, as flux is generated by two same polarity adjacent PMs, which is referred as flux focusing effect. Seeing that, this topology can increase the density of airgap flux and effective PM flux, the desired output power can be obtained by a low number of ampere-turns in the stator. Therefore, the power factor is improved by the reduction of winding reactance in this regard.

V. CONCLUSION

In this research work, DSAFST-PMVM is analyzed and compare its performance with the proposed model and optimized model. Cogging torque and torque ripples are mainly focused and reduce to the significant level without reducing the back emf and torque of the machine. The proposed notched shape magnet has the advantage of less cogging torque and torque ripples as verified by the 3D-FEM simulation results, as compared to the basic rectangular shape magnet. There is a 36.67% reduction in the cogging torque due to the proposed PM. Furthermore, optimization of the magnet shape is done to improve the performance of the machine, resulting in a further 8.53% reduction in cogging torque. Torque ripples of the basic model are 8.82% which is reduced to 4.22% by the proposed magnet shape, with optimization it further reduces to 3.93%. The low power factor (inherent problem) of the vernier machine is improved to 0.88.

REFERENCES

- [1] A. Ishizaki, T. Tanaka, K. Takasaki, and S. Nishikata, "Theory and optimum design of PM Vernier motor," in *Proc. 7th Int. Conf. Electr. Mach. Drives*, Durham, U.K., Sep.1995, pp. 208–212.
- [2] S. L. Ho, S. Niu, and W. N. Fu, "Design and comparison of Vernier permanent magnet machines," *IEEE Trans. Magn.*, vol. 47, no. 10, pp. 3280–3283, Oct. 2011.
- [3] Y. Wang, W. N. Fu, S. Niu, and X. Li, "A novel stator and rotor dual PM flux modulated machine," *Chin. J. Electr. Eng.*, vol. 3, no. 1, pp. 10–15, 2017.

- [4] M. G. Simoes and P. Vieira, "A high-torque low-speed multiphase brushless machine—A perspective application for electric vehicles," *IEEE Trans. Ind. Electron.*, vol. 49, no. 5, pp. 1154–1164, Oct. 2002.
- [5] K. Atallah, S. Calverley, R. Clark, J. Rens, and D. Howe, "A new PM machine topology for low-speed, high-torque drives," in *Proc. 18th Int. Conf. Electr. Mach.*, Sep. 2008, pp. 1–4.
- [6] J. Schuttler, H. Groke, M. Siatkowski, J. Adler, and B. Orlik, "Power-optimized symmetrizing current control with a 8.7 kNm-transverse flux generator," in *Proc. 12th Int. Conf. Optim. Electr. Electron. Equip.*, May 2010, pp. 352–357.
- [7] Y. Kataoka, M. Takayama, Y. Matsushima, and Y. Anazawa, "Investigation of magnetic pole combination in a surface permanent magnet-type Vernier motor," *J. Magn. Soc. Jpn.*, vol. 37, nos. 3–2, pp. 268–272, 2013.
- [8] S. Niu, S. L. Ho, W. N. Fu, and L. L. Wang, "Quantitative comparison of novel Vernier permanent magnet machines," *IEEE Trans. Magn.*, vol. 46, no. 6, pp. 2032–2035, Jun. 2010.
- [9] J. M. Crider and S. D. Sudhoff, "An inner rotor flux-modulated permanent magnet synchronous machine for low-speed high-torque applications," *IEEE Trans. Energy Convers.*, vol. 30, no. 3, pp. 1247–1254, Sep. 2015.
- [10] P. Bolognesi, O. Bruno, and L. Taponecco, "A switched reluctance machine for high-torque low-speed applications," in *Proc. Eur. Conf. Power Electron. Appl.*, 2005, p. 10.
- [11] M. R. Harris, "The problem of power factor in VRPM (transverse-flux) machines," in *Proc. 8th Int. Conf. Electr. Mach. Drives*, Cambridge, U.K., Sep. 1997, pp. 386–390.
- [12] A. J. Mitcham, "Transverse flux motors for electric propulsion of ships," in *Proc. IEE Colloq. New Topol. Permanent Magnet Mach.*, London, U.K., Jun. 1997, pp. 1–3.
- [13] K. Atallah and D. Howe, "A novel high-performance magnetic gear," *IEEE Trans. Magn.*, vol. 37, no. 4, pp. 2844–2846, Jul. 2001.
- [14] X. Liu, K. T. Chau, J. Z. Jiang, and C. Yu, "Design and analysis of interior-magnet outer-rotor concentric magnetic gears," *J. Appl. Phys.*, vol. 105, no. 7, Apr. 2009, Art. no. 07F101.
- [15] T. A. Lipo and A. Toba, "Generic torque-maximizing design methodology of surface permanent-magnet Vernier machine," *IEEE Trans. Ind. Appl.*, vol. 36, no. 6, pp. 1539–1546, Nov. 2000.
- [16] A. Toba and T. A. Lipo, "Novel dual-excitation permanent magnet Vernier machine," in *Proc. IEEE Ind. Appl. Conf., 34th IAS Annu. Meeting*, vol. 4, Oct. 1999, pp. 2539–2544.
- [17] L. L. Wang, J. X. Shen, P. C. K. Luk, W. Z. Fei, C. F. Wang, and H. Hao, "Development of a magnetic-gear permanent-magnet brushless motor," *IEEE Trans. Magn.*, vol. 45, no. 10, pp. 4578–4581, Oct. 2009.
- [18] F. Zhao, T. Lipo, and B. Kwon, "Magnet flux focusing design of double stator permanent magnet Vernier machine," *IEEE Trans. Magn.*, vol. 50, no. 11, pp. 1–4, 2013.
- [19] E. Spooner and L. Haydock, "Vernier hybrid machines," *IEE Proc.-Electr. Power Appl.*, vol. 150, no. 6, pp. 655–662, 2003.
- [20] R. Qu, D. Li, and J. Wang, "Relationship between magnetic gears and Vernier machines," in *Proc. Int. Conf. Electr. Mach. Syst.*, Beijing, China, Aug. 2011, pp. 1–6.
- [21] F. Zhao, T. A. Lipo, and B.-I. Kwon, "A novel dual-stator axial-flux spoke-type permanent magnet Vernier machine for direct-drive applications," *IEEE Trans. Magn.*, vol. 50, no. 11, pp. 1–4, Nov. 2014.
- [22] J. F. Gieras, "Analytical approach to cogging torque calculation of PM brushless motors," *IEEE Trans. Ind. Appl.*, vol. 40, no. 5, pp. 1310–1316, Sep. 2004.
- [23] M. Aydin, Z. Q. Zhu, T. A. Lipo, and D. Howe, "Minimization of cogging torque in axial-flux permanent-magnet machines: Design concepts," *IEEE Trans. Magn.*, vol. 43, no. 9, pp. 3614–3622, Sep. 2007.
- [24] L. Jian, K. T. Chau, and J. Z. Jiang, "A magnetic-gear outer-rotor permanent-magnet brushless machine for wind power generation," *IEEE Trans. Ind. Appl.*, vol. 45, no. 3, pp. 954–962, May 2009.
- [25] M. Takano and S. Shimomura, "Improvement of torque density of variable reluctance Vernier machine for hybrid electric vehicle," in *Proc. IEEE Energy Convers. Congr. Expo.*, Denver, CO, USA, Sep. 2013, pp. 1205–1212.
- [26] D. Fukai and S. Shimomura, "Integrated radial and dual axial-flux variable-reluctance Vernier machine," in *Proc. 40th Annu. Conf. IEEE Ind. Electron. Soc. (IECON)*, Dallas, TX, USA, Oct./Nov. 2014, pp. 682–688.
- [27] J. Li, K. T. Chau, J. Z. Jiang, C. Liu, and W. Li, "A new efficient permanent-magnet Vernier machine for wind power generation," *IEEE Trans. Magn.*, vol. 46, no. 6, pp. 1475–1478, Jun. 2010.
- [28] F. Zhao, T. A. Lipo, and B. I. Kwon, "Optimum design for a double excitation spoke-array permanent magnet Vernier machine by tooth modification," in *Proc. IEEE Annu. Summer Conf.*, Jul. 2013, pp. 631–632.
- [29] Q. Wang, F. Zhao, and K. Yang, "Analysis and optimization of the axial electromagnetic force for an axial-flux permanent magnet Vernier machine," *IEEE Trans. Magn.*, vol. 57, no. 2, pp. 1–5, Feb. 2021.

•••